Iranian Journal of Fuzzy Systems

Volume 21, Number 1, (2024), pp. 103-128

Original paper

University of Sistan and Baluchestan

Fuzzy logic inherited machine learning based maximum power point tracker for cost-optimized grid connected hybrid renewable systems

N. Sampathraja [1] and L. Ashok Kumar [2]

[1,2] *Department of Electrical and Electronics Engineering, PSG College of Technology, Coimbatore, Tamil Nadu, India - 641 004.*

nsr.eee@psgtech.ac.in, lak.eee@psgtech.ac.in

Abstract

In this article, multitrial vector-based differential evolution algorithm (MTDE) is proposed as energy and cost management controller under Time of Use (TOU) tariff in grid associated domestic PV-wind power system tied with battery storages. To enrich the energy efficiency of a proposed power system, two optimisation algorithms are proposed in the scheduling operation. TOU billing is a cost- reflective power pricing strategy that has been found as an effective way to reduce peak energy consumption in the residential segment everywhere the world, mainly in industrialised nations. In the optimisation maximizing the cost benefit of the household energy is taken as the objective and the dispatching ratio of electricity sold to the grid and used locally is treated as the optimisation variable. Using MATLAB, the performance of proposed MTDE in the aspect of daily cost benefit and revenue growth rate are presented with the comparative analysis of gravitational search algorithm and conventional self-made for self-consumed and rest for sale (SFC&RFS) mode-based energy management controller. In comparison to the SFC&RFS mode, the GSA-based cost optimization offers a 21.46% increase in revenue growth, while it is improved to 38.7% using proposed MTDE algorithm. The paper also addresses the significance of fuzzy logic based maximum power point tracking (MPPT) of solar PV in enhancing the energy management of the proposed system. The prototype of fuzzy logic MPPT for 10 W solar panel is presented and the tracked maximum power is visualized using Thingspeak IoT cloud server. The tracking speed of the MPPT can be increased by introducing machine learning algorithms at the cost of memory and complexity. In this article, the linear regression-based machine learning algorithm is implemented in the hardware prototype by utilizing the dataset aggregated from fuzzy MPPT and hence the proposed MPPT inherits the characteristics of the fuzzy MPPT with increased tracking speed. Around 75 % data are used for training, 25% of data are used to test the model and it is observed that the root mean square error (rmse) is 5.1334 and mean square error is 26.3521 and the model is utilized as MPPT for the real-time inputs.

Keywords: PV system, wind energy, energy and cost management controller, time of use tariff, MTDE, GSA, fuzzy logic MPPT for solar PV, internet of things, linear regression based machine learning.

1 Introduction

The enormous growth in electricity consumption, the exorbitant cost of fossil fuels, the desire to minimize air pollution, and the need to improve energy security all compel the construction of more competent and environmentally friendly power stations [4, 9]. Both advanced and emerging countries are attempting to increase their electricity production by utilizing renewable energy sources (RESs) [5]. Numerous renewable energy (RE) technologies have become commercially viable during the last few decades, including wind, photovoltaic (PV), solar thermal, biomass, and different forms of hydropower [2]. Despite RESs have high capital costs [4], their benefits are becoming increasingly evident as cost optimization models are developed [23]. Once the cost issue is resolved, RESs would be used to increase access to energy in evolving nations where there is a discrepancy in supply and demand [24]. Cost-effectiveness and reliable control

Corresponding Author: N. Sampathraja
Received: February 2023; Revised: July 2023; Accepted: November 2023.
https://doi.org/10.22111/IJFS.2023.44709.7874

mechanisms are critical when using renewable energy sources [15]. Solar, wind, and hydropower are the best renewable energy sources for small-scale and off-grid applications [17, 26]. As a result, relying solely on these renewable energy sources compromises the entire power system's reliability [14, 18]. This means that significant storage or hybridization with other renewable and non-renewable energy sources are required in order to deploy sustainable energy in a power system. The most feasible strategy is to combine solar and wind generation to produce electricity that is both reliable and affordable when used in an off-grid setting [1]. It will also improve system reliability and reduce reserve capacity to some extent by adding a kind of energy storage like a battery storage system (BSS) [11, 12]. While a renewable energy system coupled with a grid-connected battery provides enhanced reliability, it also reduces the size of the battery required for the same amount of power.

When it comes to grid-connected renewable energy systems for homes, there are four areas where energy efficacy can be enriched: performance; operation; equipment; and technology [3, 22, 27]. At the operational level, optimization is a frequently used methodology for improving energy efficiency. In this article, optimisation algorithms are proposed scheduling operation of considered renewable energy system to enhance the energy efficiency. Rahman et al. (2017) examined four TOU pricing models for reducing home consumers' electricity bills, taking into account various types of residential customers [21]. For grid-connected home PV power systems, Zhang and Tang in 2019 examined genetic algorithms based on TOU for the efficient and cost-effective use of PV energy [28]. Zhang and Tang employed a genetic algorithm to figure out cost profit of a TOU for a renewable energy. A well-known downside of GA owing to crossover overlap is that it achieves early convergence despite being a metaheuristic technique. To encounter the premature convergency in this article, multi trial vector-based differential evolution algorithm (MTDE) is proposed and compared with the performance of gravitational search algorithm (GSA) based energy management control in the aspect of economic benefit. GSA is a physics-based method that replicates natural physical principles. This method makes use of physics concepts and rules like gravitational pull to communicate among participants in the search space.

The MTDE method comprises of many differential evolutionary (DE) algorithm search strategies. As a result, the MTV technique is used by three diverse TVPs: representative based trial vector producer (R-TVP), local random based trial vector producer (L-TVP), and global best history-based trial vector producer (G-TVP). Many distinct and complicated problems can be solved by using these TVPs, which add variety to the search strategy. R-TVP preserves diversity, L-TVP gains from an appropriate balance of exploration and exploitation, and G-TVP has significant exploitation capabilities all at the same time. The winner-based distribution and its policy are described in MTDE based on R-TVP, L-TVP, and G-TVP behaviours to allocate the population amid them. This algorithm was developed by Mohammad H. Nadimi-Shahraki et al (2020) for engineering design challenges [19]. Mohammad H. Nadimi-Shahraki et al (2020) compared the performance of proposed MTDE algorithm with various metahuristic algorithms like GWO, WOA, SSA, HHO, CoDE, EPSDE, QUATRE and MKE, demonstrated that the MTDE algorithm offered improved performance and benefits from high accuracy of optimal solutions obtained. Since GSA is not compared with MTDE, so it is considered as power and cost management controller in this analysis. Hence in this research to attain maximum economic benefit MTDE algorithm is proposed as intelligent energy management controller.

Hemalatha and Seyezhai (2023) analysed AI-based MPPT using a fuzzy algorithm is proposed for the grid-tied PV system and its functionality under constant irradiance and variable uniform irradiance [8, 13]. Tracking performance of fuzzy MPPT is tested in hardware for real-time implementation. Gómez-Lorente et al (2022) studied Multiple Linear Regression based MPPT for DC load connected PV system. Linear Regression based MPPT is analysed under various irradiance conditions such that constant, step change and linear change. Effectiveness of machine learning in MPPT is validated with variable irradiance and temperature [10]. From the survey it is observed that both AI-fuzzy and Linear Regression are effective MPPT methods [25]. Hence in this article to attain maximum performance in MPPT fuzzy is hybridized with Linear Regression and proposed as MPPT in PV system.

The organization of the article is as follows: Section 2 presents the model of a grid-connected hybrid renewable energy system. Section 3 formulates the cost optimization problem for the proposed model, considering the time of use tariff. It also discusses the implementation of two algorithms: the GSA algorithm and the MTDE algorithm. Section 4 provides an analysis of the results and presents the findings related to cost benefit and economic growth achieved by the proposed algorithms. Sections 5 and 6 focus on the PV system within the proposed hybrid renewable sources. In Section 5, a hardware prototype is used to implement the fuzzy logic MPPT controller. In Section 6, the linear regression machine learning MPPT is implemented, which incorporates system knowledge obtained from the fuzzy logic MPPT.

2 Grid connected renewable energy system coupled with energy storage

The proposed configuration utilizes a standard DC link to coordinate the DC output from the wind turbine, solar PV plant, and batteries. In order to convert this DC power into AC power, a typical inverter that can handle combined AC capacity is used. An overview of the proposed method is illustrated in Figure 1. For voltage matching, a DC-DC converter connects the DC buses of the wind and solar PV plants with batteries. To charge the batteries from the DC bus, a DC-DC buck converter is used. Inverter with a low-pass filter (LCL) is used to convert the DC to AC and to shape the sine wave with reduced harmonics. Figure 1 shows that Energy Management System is controlling all the power sources, battery charging, discharging, grid integrating and load. The Solar power is injected to DC bus using a boost converter. The maximum power is extracted from the solar panel using MPPT algorithms. The MPPT algorithm produces duty ratio for the DC to DC converter to operate the panel at maximum power point.

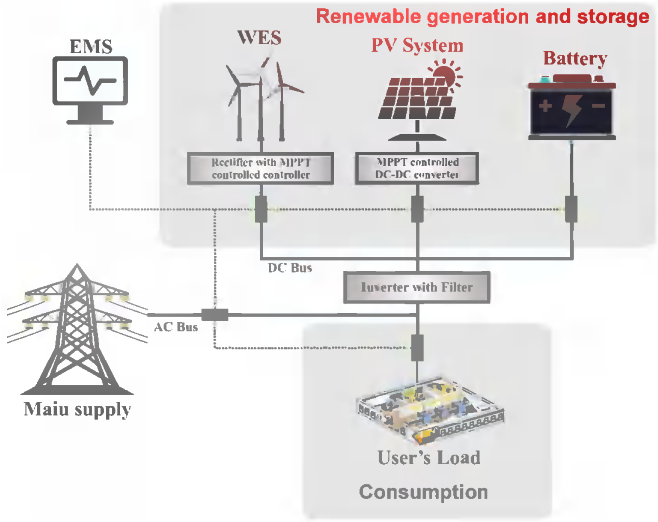

Figure 1: An overview of the proposed method.

The utilization of a fuzzy logic MPPT controller for solar PV system is proposed in this work, aiming to achieve the duty ratio for DC-to-DC Converter. The application of the Mamdani method in fuzzy logic involves two inputs, namely change in power and change in voltage and change in duty ratio is the output variable. Each input variable is characterized by five membership functions, while the output variable is characterized by nine membership functions. The determination of the duty ratio involves the incorporation of 25 rules into the fuzzy inference system.

A 6-kW wind energy conversion system consists of wind turbine and permanent magnet synchronous generator (PMSG), three-phase diode bridge rectifier and a DC-DC boost converter. The low operational and maintenance costs of a permanent magnet synchronous generator are factors in the decision. WECS should match the DC bus voltage and to achieve this couple of PI regulators are employed. The DC voltage error is dealt with outer PI controller, which generates a current reference. The duty ratio is generated by the internal PI controller, which deals with the current error. The generated PWM signal from PI controller triggers the switch of Boost converter to get the desired voltage.

The DC bus ties the solar, wind, and battery systems. The load and grid are connected to the DC bus via an inverter and filter unit. Energy Storage System (ESS) consists of four 12V, 65AH batteries connected in parallel. ESS is connected to the DC bus through two converters because the DC bus has a rating of 680V. A buck converter charges the battery, and a boost converter discharges it. An energy management controller regulates the power going to / coming from each converter. EMC governs the state of charge (SOC) of battery to prevent overcharging and deep discharging, there by extending the life of battery. The inverter and grid are connected via a three-phase LCL filter for optimal performance and ease of modelling.

3 TOU tariff-based smart energy and price management system

In general management of power system is scheduling of sources based on power availability and demand, whereas in proposed system tariff is the one more key parameter decides the energy efficiency.In these modes of operation, the cost

of power is divided between the cost of buying power (from the grid) and the cost of selling power (to the grid). So, the cost and power of Figure 1 systems are shown as follows:
The entire advantage of a grid-associated domestic energy system on the period, $[t_0, t_f]$, is as below

$$Cost_{entire-TOU} = \int_{t=t_0}^{t_f} (Cost_{sell,t} - Cost_{buy,t}).d(t). \tag{1}$$

Where t_f is the period of specimen,$Cost_{sell,t}$ and $Cost_{buy,t}$ are the sale and purchasing cost of energy.$Cost_{sell,t}$ is expressed as

$$Cost_{sell,t} = (Power_{ren,t} - Power_{L,t}).\omega_t.Cost_0. \tag{2}$$

The energy management problem's optimizing factor ω_t is the dispatching ratio. Non-conventional power produced and load mandate are $Power_{ren,t}$ and $Power_{ren,t}$,while benchmarking price of green energy is $Cost_0$. In order to keep the dispatching ratio at a minimum,

$$0 \leq \omega_t \leq 1. \tag{3}$$

The energy cost, $Cost_{buy,t}$ is influenced by the electricity tariff. It is attained by

$$Cost_{buy,t} = P_{G,t}.Cost_{price,t}. \tag{4}$$

Where $P_{G,t}$ is the power procured from the network and $Cost_{price,t}$ is the energy tariff at t. At this time, $Cost_{price,t}$ tracks a TOU tariff regulation.The entire energy price, $Cost_{entire-TOU}$ is measured as the objective role of the energy and price administration optimisation function. Maximising $Cost_{entire-TOU}$ results in the greatest possible profit for the entire microgrid.

A small power system operating in the real world is subject to a number of different network feasibility and security restrictions. The following list outlines the limitations associated with the energy and price administration optimisation problem.

When the nonconventional power is greater than demand, i.e.,($Power_{ren,t} > Power_{L,t}$), according to the planning guidelines presented above, the battery storage system is currently in the charging condition. To be specific, the battery storage works as a load instead of source ($-Power_{BAT,t}$). Then, remaining part of excess power is further selling to grid through ω_t. As a result, the power balance should be altered as follows:

Because of the foregoing planning principles, battery storage is in a charging condition when renewable energy is more than load, i.e.($Power_{ren,t} > Power_{L,t}$). More particularly, the battery storage serves as a load instead of supply ($-Power_{BAT,t}$). Next, the remainder of the extra electricity is sold back to the grid via ω_t. The following changes should be made to the power balance as a result:

$$Power_{ren,t} = Power_{L,t} + Power_{BAT,t} + Power_{SELL,t}, \tag{5}$$

$$-Power_{BAT,t} = (Power_{ren,t} - Power_{L,t}).(1 - \omega_t), \tag{6}$$

$$Power_{SELL,t} = (Power_{ren,t} - Power_{L,t}).(\omega_t). \tag{7}$$

Where $Power_{BAT+}, Power_{BAT-}$ are the discharging power and charging power, respectively.Batteries enter a discharging state when renewable energy is larger than the load, i.e.,($Power_{ren,t} < Power_{L,t}$). To match the load demand, more electricity will most likely be purchased from the grid. In this case, the system balance is stated as follows:

$$Power_{L,t} = Power_{G,t} + Power_{ren,t} + Power_{BAT,t}. \tag{8}$$

Deep discharging or overcharging a battery reduces its useful life and increases the cost of maintenance. As a result, the following battery energy storage limits are logical.

$$Power_{BATMIN} \leq Power_{BAT,t} \leq Power_{BATMAX}, \tag{9}$$

where the energy stored in the battery is $Power_{BAT,t}$ at t. $Power_{BATMIN}, Power_{BATMAX}$ makes a limit for $Power_{BAT,t}$. Consolidating the objective function 1 and constraints,finally obtained as the energy management optimisation problem

under TOU tariff as follows [28].

$$\begin{aligned}
&maxCost_{entire-TOU}(\omega_t) = \int_{t=t_0}^{t_f} (Cost_{sell,t} - Cost_{buy,t}).d(t),\\
&Power_{G,t} + Power_{ren,t} + Power_{BAT,t} - Power_{SELL,t} - Power_{L,t} = 0,\\
&(Power_{ren,t} - Power_{L,t}).(1-\omega_t) + Power_{BAT,t} = 0,\\
&(Power_{ren,t} - Power_{L,t}).(\omega_t) - Power_{SELL,t} = 0,\\
&0 \le \omega_t \le 1,\\
&Power_{BATMIN} \le Power_{BAT,t} \le Power_{BATMAX},\\
&Power_{BAT+} \le \frac{0.2E}{\Delta t},\\
&Power_{BAT-} \le \frac{0.2E}{\Delta t}.
\end{aligned} \tag{10}$$

The above power and cost management optimisation in equation 10 is a constrained nonlinear optimisation problem. Additionally, it is first and primarily digitised before being addressed mathematically. The predicted renewable and residential load power is an input to the energy management issue, and the optimisation parameter is the dispatching ratio ω_t, which is optimized using the MTDE algorithm.

3.1 Gravitational search algorithm based energy and cost management controller

Various heuristic advancement strategies have been developed recently. A large number of these tactics are offered as advancement estimates based on the law of gravity and mass linkages [22]. GSA has a few points of interest that highlight its significance in comparison to other naturally invigorated systems. To begin with, it only involves the modification of two parameters: particle mass and velocity, and it has the ability to find a nearly global optimum solution. The GSA differs from previous nature-inspired algorithms in its ability to find a nearly global optimum solution.The searcher expert in the suggested computation are an aggregation of masses that are connected to one another based on Newtonian gravity and movement laws. The proposed method was compared to some well-known heuristic algorithms [27]. The obtained findings support the proposed technique's superiority in lighting various nonlinear capacities.

3.1.1 Algorithm for GSA

Step 1: (initialization)
Current position: position of particles
Velocity, Acceleration, Mass
Force : the gravitational force among the particles
Dim : length of test functions
N : number of particles
G_0 : gravitational constant
Min, Max: search space boundaries

Step 2: Read the parameters of the system under consideration. Such as PV power, wind power, load power, battery power and tariff. Estimate the difference in power and decide the state of battery like charging or discharging. Similarly decide state of grid power buying or selling.

Step 3: Evaluate the fitness of agents.

Step 4: Update G(t), best (t), worst (t) and $m_i(t)$ for $i = 1, 2, \cdots x$,

$$G(t) = G_0 e^{-\frac{\alpha t}{T}}. \tag{11}$$

Where G_0 and α are initialized in the beginning of the search and their values will be reduced during search. T is the total iteration

Step 5: Compute total force for diverse directions.

The gravitational force $F_ij = G\frac{M_{aj}M_{pi}}{R^2}$, where M_{aj} and M_{pi} are active and passive masses of the object j and i respectively

Step 6: Compute acceleration and velocity

$$a_i = \frac{F_{ij}}{M_{ii}}, \qquad V_i(t+1) = rand_i * a_i(t). \tag{12}$$

Where M_{ii} is inertial mass of agent i

Step 7: Update particles position.

$$X_i(t+1) = rand_i * V_i(t) + a_i(t). \tag{13}$$

Step 8: Repeat steps (3) to (7) until stopping criteria is reached.

Step 9: End of iteration.

The Number of agents is taken as 30, Initial G_0 is 100 and the maximum generation T is assigned as 50.

3.2 MTDE algorithm-based energy and cost management controller

The suggested MTDE algorithm,as illustrated in Figure 2, has two key steps: initialising and moving, both of which are based on the MTV method.N individuals $x_1, ..., x_N$ are randomly dispersed in the search space in the initialising step to examine a constrained boundary between lower bound (l) and upper bound (u).

$$X_{ij} = l_j + (u_j - l_j) * rand(0, 1). \tag{14}$$

Where x_{ij} is the i-th individual's position in j-th dimension, l_j and u_j are the lower and upper bound of the j-th dimension. There are D dimensions to the search space, therefore the individual x_i is shown as a vector $x_i = x_{i1}, x_{i2}, \ldots, x_{iD}$. N individuals are held in a matrix XN×D. $f(x_i)$ calculates each individual's fitness level and the g_best is the one with the highest fitness level. Read the parameters of the system under analysis such as PV power, wind power, load power, battery power and tariff. Estimate the difference in power and decide the state of battery like charging or discharging. Similarly decide state of grid power buying or selling. The movement step is described in the following subsection in detail since it is the main part of the MTDE algorithm.

3.2.1 Movement step using MTV approach

Movement in the MTDE process is based on three trial vector producers and the above-discussed MTV methodology: representative based trial vector producer (R-TVP), local random based trial vector producer (L-TVP), and global best history-based trial vector producer (G-TVP). By combining these three trial vector producers, MTDE will be available to address any problems. With regard to preventing and maintaining diversity, R-TVP is particularly useful.With regard to exploration and exploitation, L-TVP benefits from fast convergence and a correct balance, and G-TVP represents a significant ability in escaping the local optima.The MTDE algorithm's movement step has four substeps, as shown in Figure 2 : winner-based distributing, multi-trial vector creating, assessing, and life-time archiving. Assumed k WinIter, each with n iterations, and solitary one winner TVP signified by Win-TVP for each WinIter. The winner based distributing substep uses the distribution policy to allocate the population across the trial vectors R-TVP, L-TVP, and G-TVP after determining the Win-TVP. A random member of the union population and two individuals are used in the R-TVP to move the individual populations out of local optima while retaining variety. As a result of learning from both its subpopulation members and other members of the union population, L-TVP enjoys rapid convergence while also maintaining a healthy balance between exploration and exploitation. While R-TVP relies on evolutionary learning, final trial vector u_i uses individual learning rather than crossover. gbest-history is the history of gbest and it is used in G-TVP to overcome the problem of trapping in local optima.

A key feature of the G-TVP is the ability to learn from several different gbests from the gbest-history, which is meant to store the H numbers of the best-obtained individuals thus far. This memory serves as a repository for previously investigated areas of the search space where successful solutions have been discovered. gbest-history is initialised with just the gbest in the first iteration. The gbest of each iteration is then added to the gbest-history separately in subsequent iterations. After all previous gbests have been accounted for, the current gbest will be replaced with the gbest with the highest fitness value. The quality of each trial vector from UX-TVP is compared to its matching individual population from XX-TVP in the evaluating substep. If $f(u_i) \geq f(x_i)$, then x_i remains unaltered in the population,

as shown in Figure 2, where $f(x_i)$ is an individual population fitness function and $f(u_i)$ is a union population fitness function.

Alternatively, the population updating mechanism changes the position of x_i by u_i, if it might be better, i.e., $f(u_i) < f(x_i)$. In addition, the number of people helped by each TVP is increased by one, and the scale vector (F_i) value is saved. Then, as an inferior solution, the life-time archiving substep adds x_i to the life-time archive.

The life-time archive is initially empty, and it can store the position and lifetime of N persons. The lifespan of archived individuals is increased by one at the conclusion of each iteration, while N younger archived individuals with shorter lifetimes are kept. Finally, the iteration counter (iter) is raised by one, and the evolutionary search can be repeated until the maximum number of iterations (MaxIter) is reached.

Table 1: Specification of the proposed system

System	Specification
PV.	4.5 kW
Boost converter for PV	
Inductor	100μH
Capacitor	1000μF
Switching Frequency	20kHz
Wind	6 kW
Boost converter for Wind	
Inductor	110μH
Capacitor	1000μF
Switching Frequency	20kHz
Battery	3 kW
DC Bus	680 V, DC.
Inverter	3ϕInverter, 50 Hz, 410 V

4 Simulation results and analysis

In order to model a grid-connected PV-wind system, MATLAB/Simulink is employed. Specifications for the proposed system are shown in table 1. In the case of PV systems with fuzzy MPPT and WECS systems with TSR MPPT, the hourly weather profile of Tamilnadu is taken into account.

MATLAB/Simulink is used for energy management analysis to examine the maximum power produced by PV and wind systems. In practical to validate economic benefit of proposed system, considering two months data is advisable since in Tamilnadu energy billing is calculated by bi monthly. Two months of hourly profile is a huge data for analysis therefore in this article one week data is assumed for analysis.

The initial value of battery is assumed as 3000 W. For one week, the financial advantages of a system based on GSA and MTDE are examined. Figure 3 depicts the hourly profile of wind power using TSR MPPT for one week. It is noted that, for all the considered days, the wind power curve is always higher than 1000 W.

It is observed that, for each day, the wind produces the maximum power at 9 PM and the minimum power at 9 AM. On each day, the wind produced more than 3000 W of power at 5 PM, 8 PM, 9 PM, 10 PM, and 11 PM respectively. On day 7, the maximum power of the wind is 4073 W and the minimum power is 1365 W. It has been determined that the wind produces 50% (3000 W) of its power generation capacity every day, and more than 3000 W five times per day, for a total of 35 times per week.

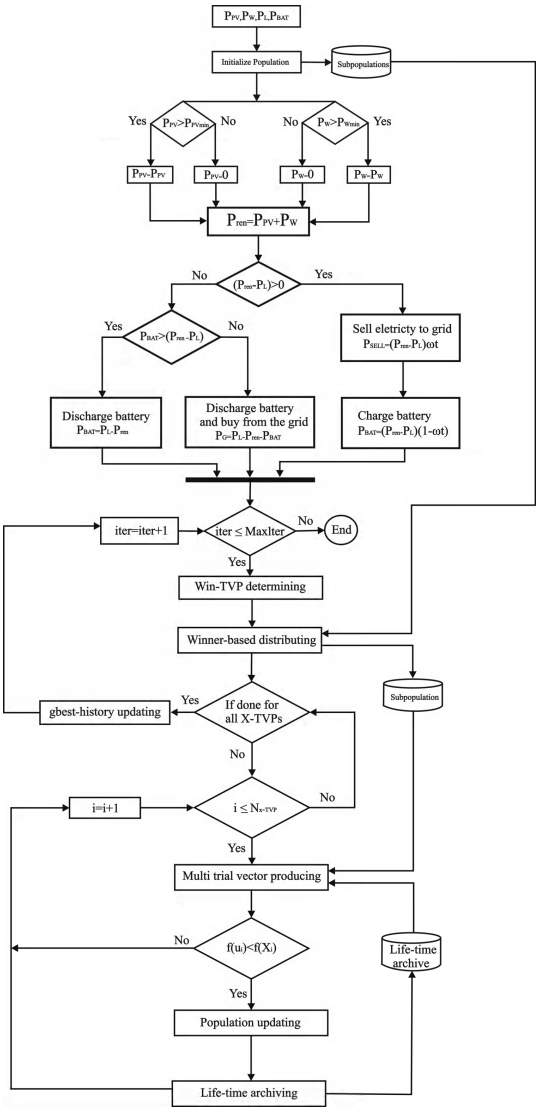

Figure 2: Flowchart of MTDE algorithm.

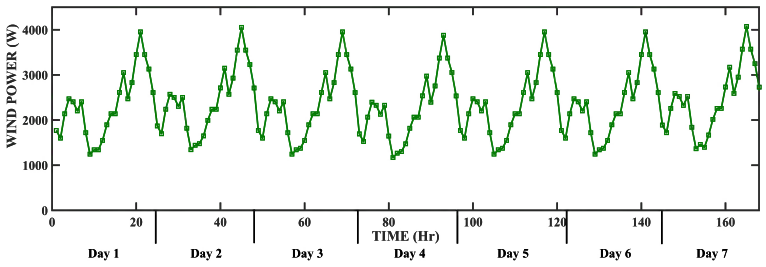

Figure 3: Hourly profile of wind power for one week.

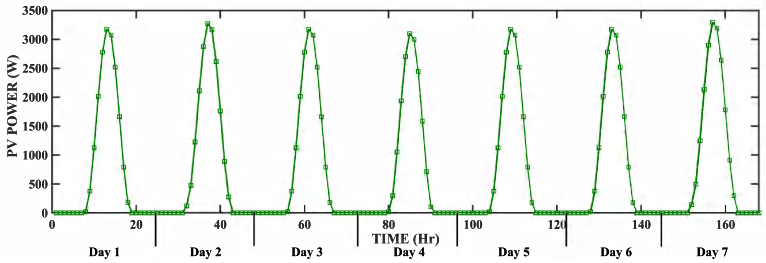

Figure 4: Hourly profile of PV power for one week.

Certainly, the maximum wind power produced is 4073 W on day 7 and the least power produced by the wind is 1170 W on day 4.

Figure 4 shows the 1-week PV power plot.It is noted that in the absence of radiation during 1 AM to 7 AM and 7 PM to 12 AM, the PV produces nil power. During 6 PM on day 2 and day 7, the PV power is greater than the non-significant power, whereas on days 1,3,4,5, and 6, the PV power is non-significant. But in the case of 8 AM, PV powers are non-significant for all considered days. It is noted that on each day the PV produces its peak power at 1 PM, and also, on each day the PV produces more than 3000 W of power at 1 PM and 2 PM.
It was observed that every day the PV produced 50% (2000 W) of its power generation capacity, and twice a day it produced more than 3000 W. The maximum PV power produced is 3290 W on day 7 as shown in Figure 4.

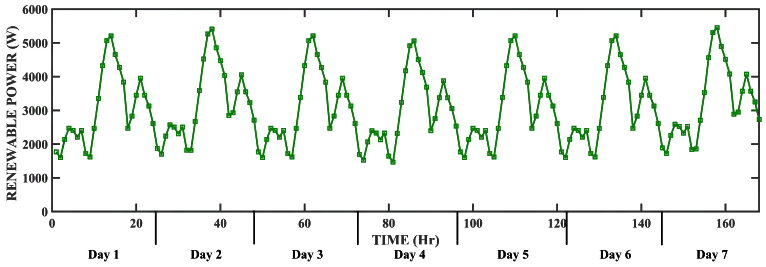

Figure 5: Hourly profile of renewable power for one week.

The renewable power curve is shown in Figure 5. The integration of PV and wind power is renewable power. The PV and wind power are summed only if the PV and wind power are above the considered minimum value. If any of the PV or wind power is below the minimum, then the PV or wind power is considered as zero for that specific time. It is noted that renewable power never goes below 1000 W, because of wind power. Simultaneously, renewable energy reaches its peak value when PV reaches its peak value.

Figure 5 shows that the maximum and minimum renewable power for each day are at 2 PM and 2 AM, respectively, but on day 4, the minimum renewable power is at 9 AM. It is analysed that the renewable power is low from 1 AM to 9 AM. This is due to the insufficient PV power at that time, so only wind power is considered. Whenever the PV power is greater than 3000 W, the renewable power reaches above 5000 W. When the wind power is at its maximum, i.e.,4073 W (on day 7 at 9 PM), the renewable power is also the same at that time, because the PV power is non-significant at the time, the wind power alone is considered as renewable power. When the PV power is at its peak, i.e., 3290 W on day 7 at 1 PM, the renewable power at that time is 5305 W.

The maximum renewable power achieved is 5450 W at 2 PM on day 7. At that period, the PV power is at 3190 W and the wind power is at 2260 W. The least renewable power is 1468 W, which is on day 4 at 9 AM. Here the PV and wind power are 298 W and 1170 W, respectively. Furthermore, renewable power has 50% (5000 W) of its power generation capacity, and produces more than 5000 W twice a day.

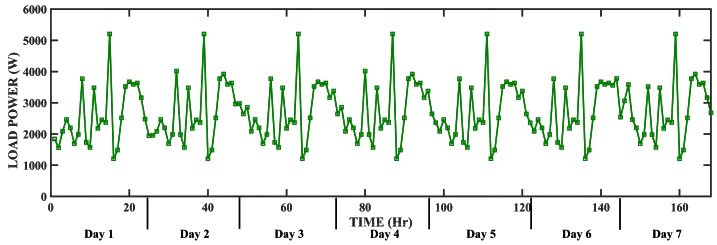

Figure 6: Hourly profile of load power for one week.

Figure 6 illustrates the load curve for one week. It is seen that every day, between 8 AM, 11 AM, 3 PM, and 7 PM to 11 PM, the load power is above 3000W. Every day, the load power reaches its peak power of 5203 W at 3 PM and its lower value, i.e., 1209 W, at 4 PM. It is also noted that during day 1 to day 6, at 8 AM, the load power is higher than renewable power, so at these times, demand power is much higher than at other hours.

4.1 Results and analysis of the energy and price management system based on GSA under the TOU tariff

This section examines the GSA-based energy and price managing system with the TOU rate in terms of the dispatch ratio, battery power, and cost. Figure 7 shows GSA's dispatch ratio for 1-week. The value of the dispatch ratio decides the charging and selling ratio of the battery and its cost. During the low tariff periods (1 AM to 7 AM and 10 PM to 12 AM), the demand is purchased from the grid. At that time, the dispatch ratio is zero. From the Figure 7, it is seen that the dispatch ratio is 1.

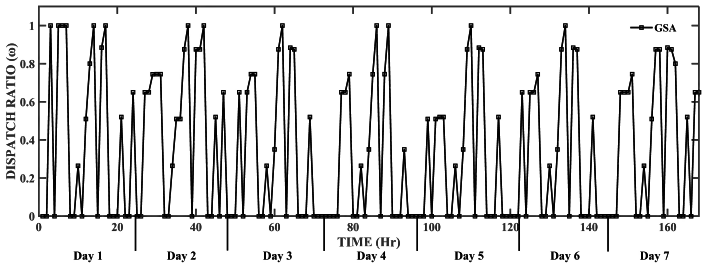

Figure 7: Dispatch ratio using GSA for one week.

This is because the battery has enough power, so the battery does not need to be charged, and then the excess power can be sold to the grid. In some cases (except on low tariffs), the dispatch ratio is 0. This means that either the battery or renewables will meet the load or purchase the power from the grid. If the dispatch ratio is greater than zero, then the battery gets charged and sells the excess power to the grid. For instance, at 6 PM on day 4, the load power is 2517.335 W, the renewable power is 2397 W, and the battery power is 2828.631 W. Here the dispatch ratio is zero, since the load power is greater than the renewable power, there will be a 120.355 W demand that is present, so this demand is supplied by the battery.

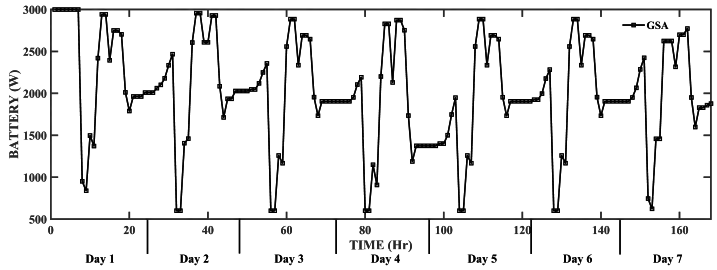

Figure 8: Battery power using GSA for one week

Figure 8 shows the battery plot for 1-week. Initially, the battery is at full capacity, i.e., 3000 W and the battery gets discharged whenever the renewable power alone doesn't meet the load. The battery is charged only when the renewable power is greater than load power. The charging ratio of the battery is decided by the dispatch value. If the battery has 90% of its total capacity, then charging of the battery does not take place. Moreover, the discharging of battery power is limited to 20% of its full capacity. The power is purchased from the grid to meet the load when the battery is 20% of its capacity. It is seen that under low tariff conditions, the power is purchased from the grid so that the battery is not discharged to meet the demand. This strategy is economically efficient by reducing the purchasing cost at a high tariff as the stored battery power could be able to meet the load at that time. Considering day 4 at 6 PM, the load power is greater than renewable power, so the demand power (120.355 W) is supplied by the battery, hence the dispatch ratio is zero at this time. After supplying the demand, the battery power reduced from 2873.326 W to 2725.991 W, as shown in Figure 8. It is noted that in any case, the battery is always above its 20% rated capacity. The hourly profile of cost is shown in Figure 9.

The cost is entirely dependent on renewables, load, battery power, dispatch ratio, and tariff. It is noted that on in-between days the cost is negative. This is because of either a low tariff or low renewable power at that time. Due to this, the power is purchased from the grid. The cost curve is positive at certain hours;this is due to the renewable power alone meeting the load, so the excess power is used to charge the battery or sold to the grid. In some cases, the cost curve is zero. This means that the renewables can't meet the load alone, so there is no excess power. Only demand power is present, so the battery is taken into account to supply the demand. For instance, on day 4 at 6 PM, there is no excess power present, only demand, so the selling cost is zero at this time. Similarly, on day 6 at 2 AM, only demand power is present. Due to the low tariff at this time, the demand power is purchased from the grid. The buying cost is (difference in load and renewable power) $*$ tariff price, so this time the purchasing cost is 5.4055 INR. It is observed that the maximum buying cost is 9.5293 INR on day 7 at 2 AM and the peak selling price is 8.6546 INR on day 7 at 2 PM.

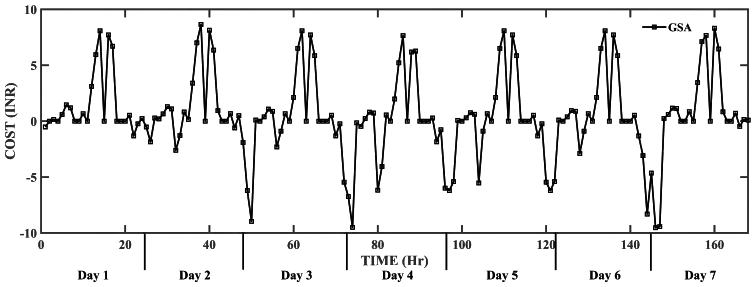

Figure 9: Cost using GSA for one week

4.2 Results and analysis of the energy and price managing system based on MTDE under the TOU tariff

The performance of the MTDE-based energy and price managing system with the TOU rate is analysed in terms of dispatch ratio, battery power, and cost, which are discussed in this section. The hourly based profile of the dispatch ratio for MTDE for 1 week is presented in Figure 10.

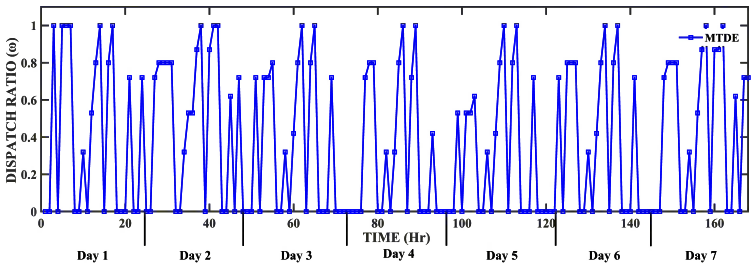

Figure 10: Dispatch ratio by MTDE for one week

On day 4 at 6 PM, it is seen that the dispatch ratio is zero, because the load power is greater than the renewable

power, so the demand power of 120.355 W is present. Here the battery power is 2828.631 W, so the battery is discharging its power to supply the demand. In the second case, on day 6 at 2 AM, the dispatch ratio is zero since the load is greater than renewable power. Even though the battery could be able to supply the demand, the tariff price is low at this hour, so instead of discharging the battery, the demand power is acquired from the network.

Figure 11 illustrates the battery power plot for 1-week. On day 4 at 6 PM, it is seen that the dispatch ratio is zero and the battery power reduced from 2828.631 W to 2708.296 W to supply the demand power of 120.355 W. Considering day 6 at 10 AM, excess power of 895.24 W is present, and the battery is less than its charging capacity, so this excess power is supplied to both the grid and the battery based on dispatch ratio, i.e., 0.32.

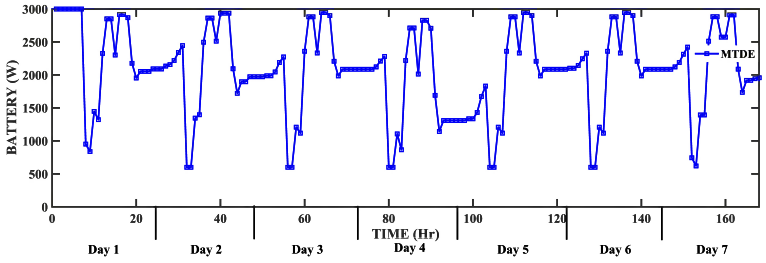

Figure 11: Battery Power by MTDE for one week

The charging of the battery is (1-dispatch ratio) * difference in load and renewable power. Based on this, the battery is charged from 600 W to 1208.764 W and the remaining excess power is sold to the grid. In any case, the battery is always above its 20% rated capacity, as shown in Figure 11. Figure 12 shows the hourly based profile of cost using MTDE.On day 4 at 6 PM, the dispatch ratio is zero since there is no excess power, only demand. This demand is supplied by the battery, so the selling cost at this time is zero. On day 6 at 2 PM, the battery is above its charging capacity, i.e., 2881.665W, and renewable power is greater than load power, so the dispatch ratio is 1. Hence, the surplus energy is traded to the grid alone. The cost benefit for this hour is 8.0846 INR. From the Figure 12, it is observed that the highest selling cost is 8.7686 INR during 2 PM on day 7 and the highest purchasing cost is 9.5293 INR on day 7 at 2 AM.

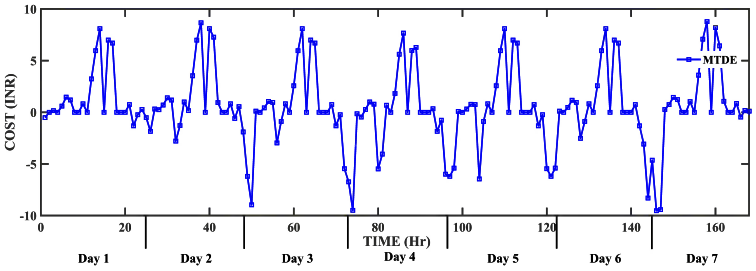

Figure 12: Cost by MTDE for one week

4.3 Comparative analysis GSA and MTDE based energy and price managing system with TOU tariff

The hourly based profile of comparative dispatch ratio plot of GSA and MTDE is shown in Figure 13. Figure 13 shows the comparative dispatch ratio of MTDE and GSA for a 1-week curve. On day 6 at 10AM, excess power 895.24W is present and also battery power is less than its capacity for both MTDE and GSA. So, the dispatch ratio must be greater than zero. The dispatch ratio of GSA is 0.263, whereas the dispatch ratio of MTDE is 0.32. From this, it is seen that in this case, the MTDE performance is better than the GSA. In the last case, the excess power of 2836.7W is present and the battery power is 2885.68W for GSA and 2881.66W for MTDE. Both the battery powers are the charging capacity, so the battery need not be charged for both. Therefore, the dispatch ratio for both the MTDE and GSA is 1, which means that excess power is sold to the grid alone. In this case, the MTDE and GSA performance are the same.

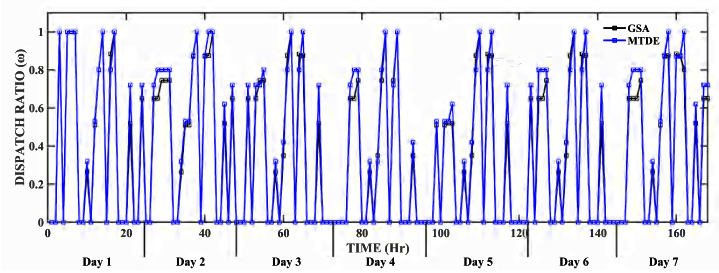

Figure 13: Comparison of dispatch ratio by MTDE and GSA for 1-week

Figure 14 illustrates the comparative battery power plot of MTDE and GSA for 1-week. On day 6 at 10 AM, it is seen that the excess power of 895.24 W is present and the battery is also less than its charging capacity for both MTDE and GSA.At this time, the dispatch ratio of MTDE and GSA is 0.32 and 0.263. Both charging the battery and selling power are done for both MTDE and GSA. Based on the battery charging term, 659.7918 W of power from the excess power of 895.24 W is used for charging the battery. As a result, the battery power rises from 600W to 1258.91W. In MTDE, the 608.7632 W of power from the excess power of 895.24 W is given to the battery. After charging, the battery power increases from 600 W to 1208.76 W and the remaining power is sold to the grid. From Figure 14, it is observed that the battery power of both MTDE and GSA is always greater than 20% of the rated capacity.

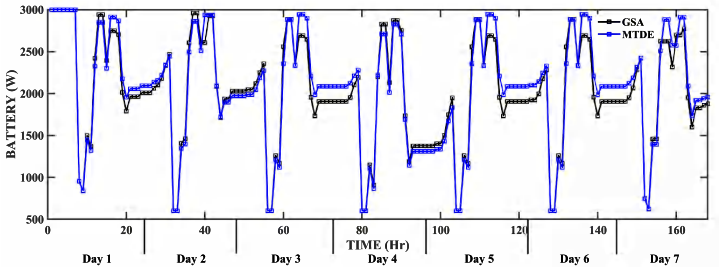

Figure 14: Comparison of battery power by MTDE and GSA for 1-week

Figure 15 portrays the hourly-based profile of the price plot of MTDE and GSA. Analyzing day 6 at 10AM, excess power of 895.24 W is present, so the surplus energy is sold to the grid, but at the same time, the battery power on MTDE and GSA is less than the charging capacity. Since the dispatch ratio of GSA is 0.263, the cost benefit of GSA is only 0.67354 INR as per the selling cost term. The dispatch ratio of MTDE is 0.32, so the cost benefit of MTDE is 0.81646 INR, which is much better than the GSA. In this case, the MTDE shows improved performance over GSA.

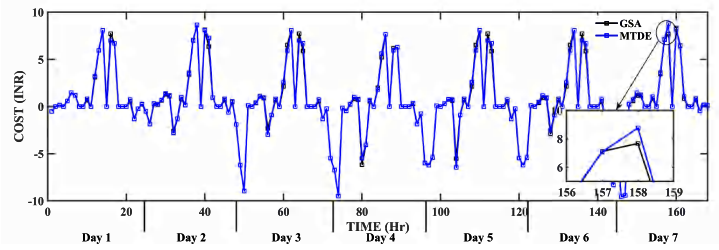

Figure 15: Comparison of cost by MTDE and GSA for 1-week

4.4 Comparative analysis over one day:

The hourly based profile of comparative performance of GSA and MTDE for day 7 is shown in Figure 16. For analysis, the 10 AM and 12 PM of day 7 are taken into consideration. In 10 AM, the renewable power is 2707 W, the load power is 1571.76W and the excess power is 1135.24 W. Since excess power is present, the dispatch ratio is greater than zero for both MTDE and GSA, as shown in Figure 16(a). As the battery power of both GSA and MTDE is less than the

charging capacity, charging is done as shown in Figure 16(b). The dispatch ratio of GSA is 0.263, so 835.57 W of power from the excess power is used to charge the battery. As a result, the boost goes from 622.617 W to 1458.19 W as shown in Figure 16(b).

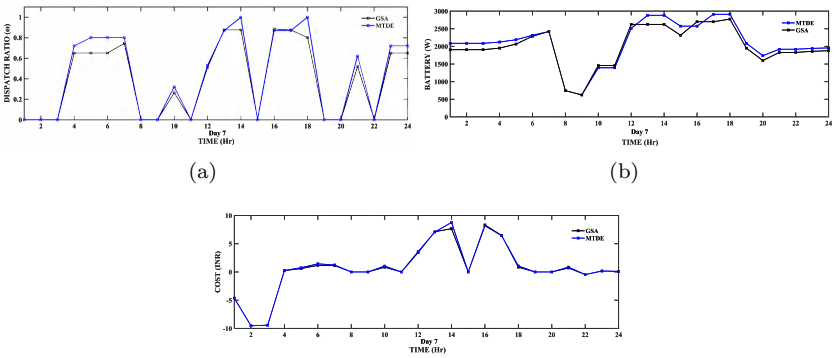

Figure 16: Comparative performance of MTDE and GSA on day 7 a) Comparison of dispatch ratio at 7th day, b) Comparison of battery at 7th day, c) Comparison of cost at 7th day.

Simultaneously, the remaining 299.66 W of excess power is given to the grid, thereby having a benefit of 0.854 INR as shown in Figure 16(c). On the other hand, the dispatch ratio of MTDE is 0.32, as shown in Figure 16(a), so the battery receives 771.96 W of excess power after charging from 622.617 W to 1458.19 W. The remaining 363.276 W of surplus energy is traded to the network with a benefit of 1.0353 INR, which is 0.1813 INR better than the GSA as shown in Figure 16 (c).

4.5 Performance analysis of proposed system using MTDE on day 7

According to Figure 17(a), power is purchased from the grid between 1 AM and 3 AM and 10 PM because the demand for power is high during these hours, so instead of discharging the battery to supply the load, energy is bought from the network since the tariff price is minimum, so the battery power can be used for supping the demand during high tariff price conditions.

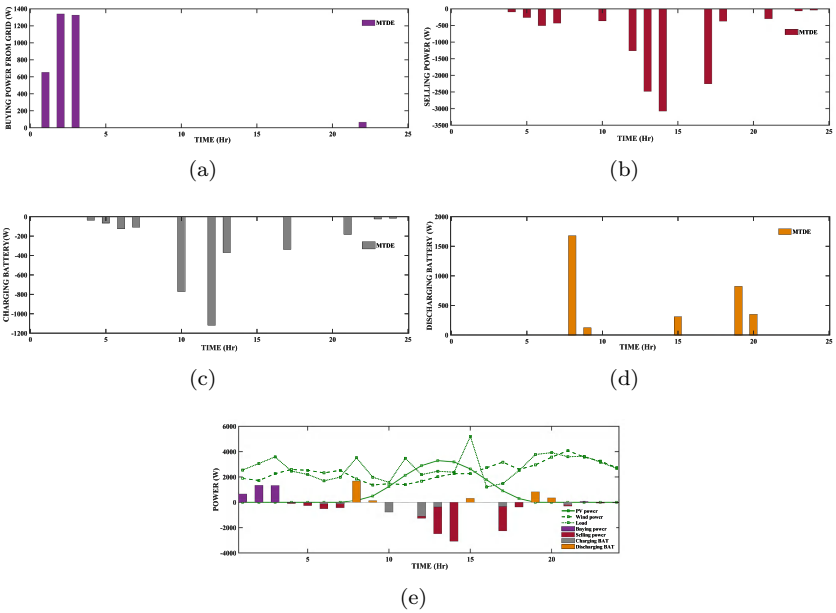

Figure 17: The performance of MTDE on day 7 a) Buying power at 7th day, b) Selling power at 7th day, c) Charging battery at 7th day, d) Discharging battery at 7th day, e) MTDE combined power at 7th day .

From Figure 17(b), it is observed that the power is sold to the grid whenever significant excess power is present. For instance, during 7 AM, excess power of 538.7703 W is present. At the same time, the battery is less than its charging capacity, so charging and selling of power takes place. With respect to dispatch ratio, i.e., 0.8, 107.771 W of the excess power is given to the battery. By this, the battery is charged from 2314.53 W to 2422.29 W, as shown in Figure 17(c). The remaining 430.9993 W of excess power is given to the grid, as seen in Figure 17(b). It is observed that during 2 PM and 6 PM the dispatch ratio is 1, since the battery has reached its charging capacity, so during these hours the excess power is given to the grid alone, as shown in Figure 17(b), and the battery is in an ideal state as shown in Figure 17(c).The Economic benefits of proposed optimisation approaches are analysed in terms of daily cost benefit and revenue growth rate. Daily cost benefit is a benefit by analysed method over a day which is expressed as

$$\text{Daily cost benefit} = \sum_{t=1}^{24} (Cost_{sell,t} - Cost_{buy,t}). \tag{15}$$

Revenue growth rate is a comparative cost benefit of optimisation approach over SFC& RFS method as shown equations 16 & 17

$$\text{Revenue growth rate}_{GSA} = \frac{\text{Daily cost benefit}_{GSA} - \text{Daily cost benefit}_{SFC\&RFS}}{\text{Daily cost benefit}_{SFC\&RFS}}, \tag{16}$$

$$\text{Revenue growth rate}_{MTDE} = \frac{\text{Daily cost benefit}_{MTDE} - \text{Daily cost benefit}_{SFC\&RFS}}{\text{Daily cost benefit}_{SFC\&RFS}}. \tag{17}$$

Table 2: Economic benefits of MTDE in comparison with GSA

Operation mode	Daily cost benefit/ INR	Revenue growth rate/%
SFC&RFS	12.183	-
GSA	14.798	21.46
MTDE	16.898	38.7

Table 2 shows the daily cost benefits and revenue growth rate of MTDE over GSA and SFC & RFS methods. From table 2, it is observed that the GSA has the daily benefit of 14.798 INR, whereas the MTDE has the daily benefit of 16.898 INR. MTDE offers an improved cost benefit of 2.1 INR compared to GSA and 4.715 INR compared to the SFC & RFS method.To validate the efficacy of proposed approach revenue growth rate of proposed system is compared with existing approach of GA analysed by Zhang and Yang (2019)[28]. Revenue growth rate of GA is similarly calculated as in equation 13. Revenue growth rate of MTDE over GSA, GA and SFC & RFS methods are shown in table 3.

Table 3: Revenue growth rate of MTDE in comparison with GSA and GA

Operation mode	Revenue growth rate/%
SFC&RFS	-
GA [28]	17.47
GSA	21.46
MTDE	38.7

From table 3, it is seen that the MTDE has improved daily benefits compared to GSA. Zhang and Tang (2019) examined that application of GA in energy and cost management improves revenue growth rate by 17.47% compared to SFC & RFS method [28]. Additionally, the use of the MTDE optimization technique accelerated revenue growth to 38.7%, while it was 21.46% by GSA compared to the SFC & RFS method. Comparative performance of MTDE over GSA, GA and SFC& RFS are shown in Figure 18. It is evident that proposed MTDE algorithm offers improve cost benefit over conventional SFC&RFS method and GSA. Meantime MTDE offers enriched revenue growth rate compared GA, GSA and SFC&RFS method.

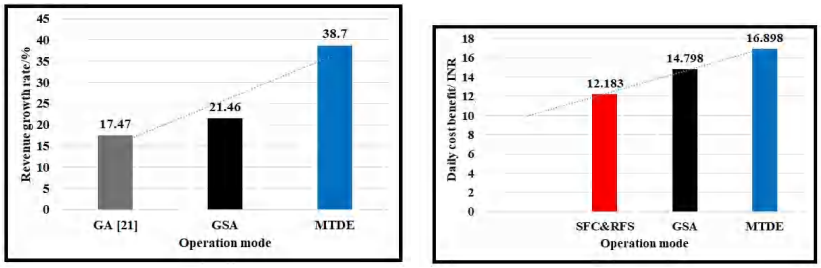

(a) (b)

Figure 18: Comparative performance of MTDE with other algorithms a)Revenue growth rate, b)Daily cost benefit

5 Fuzzy logic MPPT for solar PV systems

The efficiency of a solar panel is about 22 percent and extracting the maximum power from the panel for the given irradiance and temperature can improve the efficiency and reduces the payback period of the panel. There are various MPPT algorithms which includes Perturbation and observation (P&O), incremental conductance (INC), short circuit-method and differential method. The simplicity and ease of implementation are the advantages of hill climbing methods. The fuzzy logic based MPPT handles the non-linearities in the characteristics and does not require the mathematical model of the system [7, 16]. The fuzzy logic MPPT algorithm has reduced oscillations at maximum power point during variations in insolation and temperature because the it is unaffected by changes in circuit parameters.

5.1 Fuzzy logic MPPT controller

A Polycrystalline solar panel of 10 W with an operating voltage of 12 V is considered for the analysis. The open circuit voltage of the panel is 20.9 V and short circuit current is 0.65 A. The Vmp is 16.85 V at an irradiance of 1000 w/m^2 and temperature of 25 degree Celsius. The block diagram of the protype is shown in the Figure 19.

The Mamdani based fuzzy inference system and centre of gravity for defuzzification is used in the prototype to extract maximum power. The DC-DC buck-boost converter is used to operate the panel at the maximum power point. The change in voltage and change in power is used as an input variable to fuzzy logic MPPT controller and PWM for DC-DC converter to operate the panel in its maximum power is the output of the controller. Five linguistic variables NB

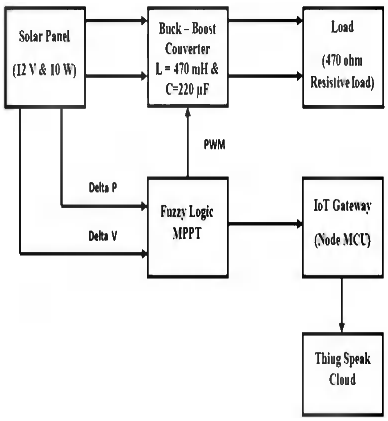

Figure 19: Block Diagram of Fuzzy MPPT of Solar PV System

(Negative big), NS (Negative small), ZE (zero), PS (positive small) and PB (positive big) are used as input membership function. Nine linguistic variables Negative Very Big (NVB), NB (Negative Big), NM (Negative Medium), NS (Negative Small), ZE (zero), PS (Positive Small), PM (Positive Medium), PB (Positive Big) and PVB (Positive Very Big) are the output membership function. The proposed FLC contains 25 rules as shown in the table 4. The fuzzy rules are build based on the relationship between input and output variables as shown in the Figure 20. At various operating

points based on change in slope in the PV curve of the solar panel the change in PWM for Buck-Boost converter is decided and shown in the following section.

Table 4: Fuzzy Rules Set of Solar PV MPPT algorithm

DelV/ Delp	NB	NS	ZE	PS	PB
NB	NVB	NM	NS	NB	NVB
NS	NVB	NM	PS	NVB	NVB
ZE	NB	NS	ZE	PS	PVB
PS	NB	NS	NS	PM	PVB
PB	NM	PS	PS	PM	PVB

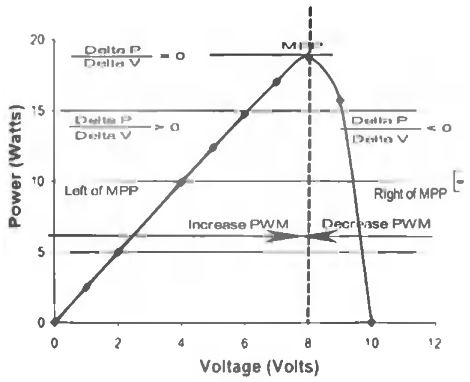

Figure 20: Relation between input variables and output variables of a Fuzzy logic MPPT controller

1. When $\frac{DeltaP}{DeltaV} > 0$ and Delta V is Positive, the operating point is in the left side and moving toward MPP. The PWM for the Buck-Boost converter need to be increased to achieve MPP
2. When $\frac{DeltaP}{DeltaV} > 0$ and Delta V is negative, the operating point is in the left side and moving away from MPP. The PWM for the Buck-Boost converter need to be increased to achieve MPP
3. When $\frac{DeltaP}{DeltaV} = 0$ the operating point is at MPP
4. When $\frac{DeltaP}{DeltaV} < 0$ and Delta V is Positive, the operating point is in the right side and moving away from MPP.The PWM for the Buck-Boost converter need to be decreased to achieve MPP
5. When $\frac{DeltaP}{DeltaV} < 0$ and Delta V is negative,the operating point is in the right side and moving towards MPP. The PWM for the Buck-Boost converter need to be decreased to achieve MPP

5.2 Implementation of fuzzy MPPT for solar PV system

The performance of the fuzzy logic MPPT has been analysed using a 10 W solar panel with a Buck-Boost converter. A resistive load of 470 ohm is used in the system and fuzzy logic MPPT is implemented using Arduino nano controller. The DC-DC buck-boost converter uses IRF9540 MOSFET switch, IN5819 diode, 470 mH inductor and 220 µF capacitor. The input current of the converter is measured using ACS712 hall effect based current sensor and it produces voltage proportional to the measured current. The input voltage of the converter is measured using voltage divider method. The analog values of measured current and voltage are given to the analog pins of Arduino controller A2 and A3 respectively as shown in Figure 21. The output voltage and output current are measured by using differential amplifier and read by the controller using the analog pins A0 and A1 respectively. The change in voltage and power are the inputs to the Fuzzy MPPT algorithm and PWM to the DC-DC converter is the output to achieve maximum power at the given irradiance and temperature.

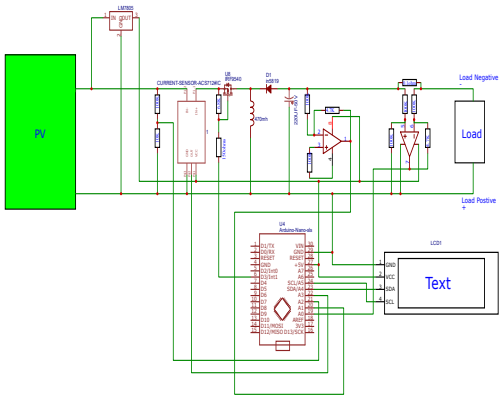

Figure 21: Circuit Diagram of Solar PV System with fuzzy logic maximum power point tracker

5.3 Data aggregation and visualization

The Thingspeak Internet of Things (IoT) platform collects, visualizes, and analyses real-time data from internet-connected sensors [6]. A private channel is created in the Thingspeak server to visualize six parameters from the Arduino controller, which include input / output voltage, current and power. The MQTT API is used to publish or subscribe to the channel from / to the device. The Arduino Nano is connected to the Thingspeak server through the ESP8266 (NodeMCU). Figure 22 and 23 shows the hardware setup and the experimental setup of fuzzy logic MPPT controller for solar PV system.

Figure 22: Hardware setup of Fuzzy Logic MPPT controller for solar PV System

Figure 23: Experimental setup of Fuzzy Logic MPPT controller for solar PV system

5.4 Results and discussion

The input and output membership function of fuzzy logic controller is shown in the Figure 24.The hardware was experimented on October 10, 2022 from 8 am A.M. to 12 Noon and the results are recorded in the thing speak cloud

server and also displayed in 16x2 LCD screen. The recorded input and output parameters are shown in the Figure 25. The voltage profile shows that DC to DC converter works in both buck mode (output voltage less than input voltage) and in boost mode (output voltage greater than input voltage) at different instant. In power profile, the input power represents the maximum power extracted from the panel and the output power is the maximum power transferred to the load. The maximum power in the experiment was recorded at 116th sample and it is around 5.5 Watts. The voltage corresponds to the maximum power point is 16.5 V which is very close to maximum power point voltage at standard test condition.The maximum peak voltage in most of the cases are ranges between 16 V and 18 V.

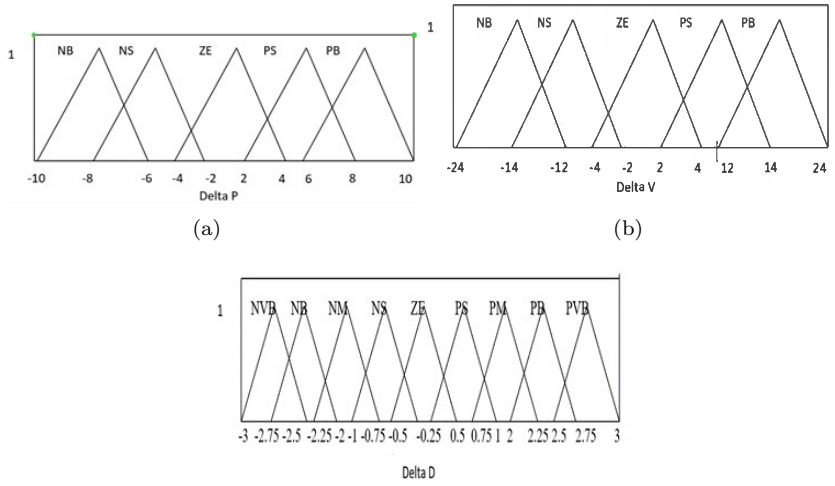

(a) (b)

(c)

Figure 24: Input and Output Membership Function of Solar PV Fuzzy Logic MPPT Controller. a)Delta P, b)Delta V, c)Delta D.

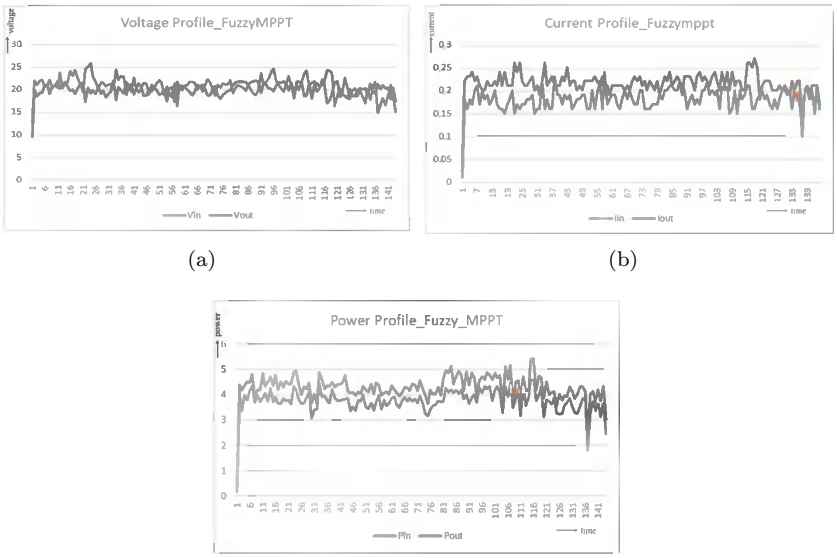

(a) (b)

(c)

Figure 25: The response of the hardware prototype of the solar PV fuzzy logic MPPT controller. a)Voltage profile, b)Current profile, c)Power profile

6 Machine learning in solar PV systems

The Machine learning algorithm has a wide application in the field of Solar PV systems which includes sizing of PV array and battery, fault detection, islanding detection, maximum power point tracking control, solar irradiance prediction, load/demand forecasting and energy generation/forecasting [26]. The Figure 26 shows the various applications of machine learning algorithm in solar PV systems. In this paper a linear regression based machine learning algorithm is adopted to track maximum power point in the solar PV system. A Linear regression is a supervised machine leaning algorithm

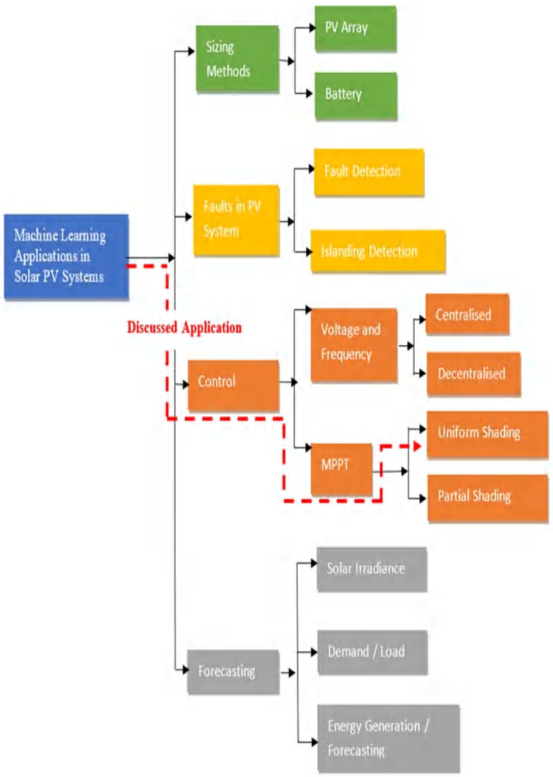

Figure 26: Applications of machine learning algorithm for solar PV systems

6.1 Linear regression based machine learning algorithm for maximum power point tracking

A linear regression-based machine learning algorithm can predict or estimates the dependent variable using an independent variable. The linear regression model develops a relationship between dependent and independent variables based on the training dataset. If the dependent variable is predicted using one independent variable, it is known as a simple linear regression.

$$Y = a + bX + error, \tag{18}$$

$$Y = a + bX_1 + cX_2 + dX_3 + ... + error. \tag{19}$$

Where Y is a dependent variable, X is an independent variable, b is the slope of the line and a is the intercept of the line. When a dependent variable is predicted based on more than one independent variables, then the model is called multi regression model. The Y in (19) is a dependent variable and, X1, X2 and X3 are the independent variables. b, c, and d are the slopes and a is the intercept of the plane. The error need to be minimized to improve the accuracy of the model.

6.2 Methodology

The Linear regression-based machine learning implemented for MPPT involves three steps, one is data collection, second is training the model using collected data and third is based on the predicted output, tuning the converter to operate the panel at maximum power point. The block diagram of the experimental setup is shown in the Figure 27. The solar panel is connected to the load through a DC-DC converter. The input voltage and input current of the DC to DC converter are taken as input features and output voltage of the converter is the output feature to be predicted.

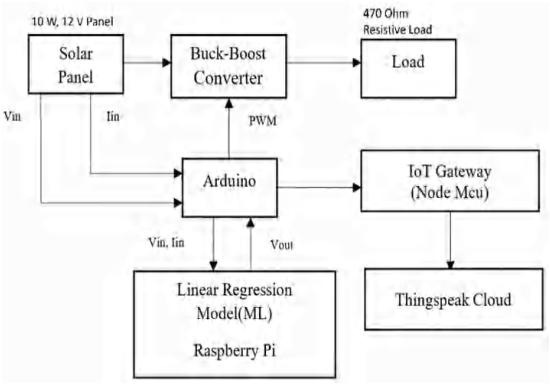

Figure 27: Block diagram of Linear regression-based machine learning algorithm for solar PV systems

6.2.1 Data collection method

The dataset was gathered during experiments using the fuzzy logic MPPT method, which were covered in Section 5. The dataset has six fields which includes input voltage, input current, input power, output voltage, output current and output power of DC-to-DC converter. About 1400 samples with 25 seconds sampling sample for a day are used for training and testing the model. The sample selection is based on the DC-DC converter operating voltage levels(system knowledge). In this work the panel voltage should be greater than 3 V to power the load. So, the recorded samples which has panel output voltage less than 3 V are to be discarded from the training dataset.

6.2.2 Training and testing

From the Dataset, 75 % of data are used for training the model and 25 % of data are used to test the model. The linear regression model on the three-dimensional plane is shown in the Figure 28.The histogram shown in the Figure 29, is created to visualize the distribution of errors and provide insights of symmetry, skewness and outliers in the error distribution. The scatter plot in Figure 30 represents a plot between actual value and predicted value and gives the better understanding of the model's accuracy. The diagonal line in the plot represents the perfect predictions.

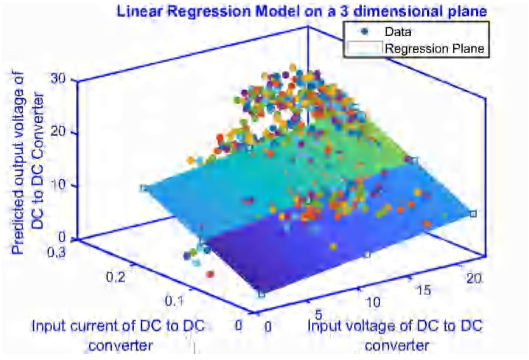

Figure 28: Three dimensional plot of Linear Regression Model

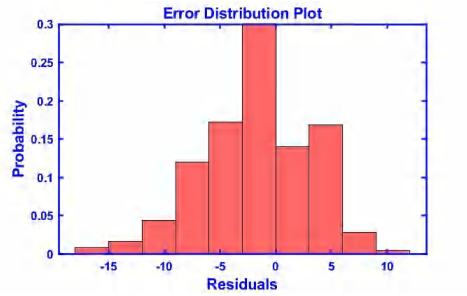

Figure 29: Error Distribution Plot

The performance of the model can be measured using mean square (MSE) and root mean square error (RMSE).

$$MSE = \frac{1}{n_s}\sum_{k=1}^{n_s}(Y_{A,K} - Y_{P,K})^2, \tag{20}$$

$$RMSE = [\frac{1}{n_s}\sum_{k=1}^{n_s}(Y_{A,K} - Y_{P,K})^2]^{\frac{1}{2}}. \tag{21}$$

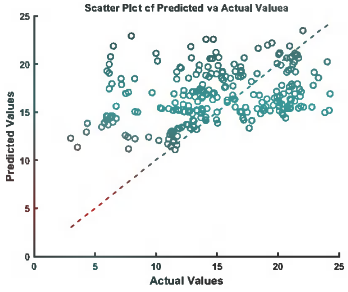

Figure 30: Scatter Plot of Predicted Value Vs Actual Value

n_s is number of samples used, $Y_{A,K}$ is the actual value of output feature from the data set and $Y_{P,K}$ is the predicted value of the ouput feature. mean square error and root mean square error represents the performance of the algorithm. Least value RMSE and MSE is the best fit to the model. It is observed that the mean square error (MSE) is 26.3521 and root mean square error (RMSE) is 5.1334. The performance of the model can be improved by increasing the training dataset and optimizing the regression coefficient. K.Rafeeq Ahmed et.al. developed a deep learning model using back propagation neural network (BPNN) to track maximum power point of the solar panel by predicting the reference voltage of maximum power point and observed the mean square error of 26.6393 which is higher than the proposed linear regression model [20]. Hence linear regression model has reduced error and best fit relative to BPNN. Also BPNN was a simulation model, but linear regression model is a real time model implemented in solar PV system.

6.2.3 Experimental setup

The block diagram for the Linear regression based mppt is shown in the Figure 31. The input voltage, current of the buck-boost converter are measured by the Arduino controller and sent to raspberry pi. The linear regression model residing in raspberry pi predicts the output voltage of the converter back to Arduino through serial communication. The logic inside the Arduino will generate the PWM for DC-DC converter to achieve the predicted output voltage of the converter. The input and output parameters of DC- DC converter are aggregated to thingspeak cloud server for the reference.

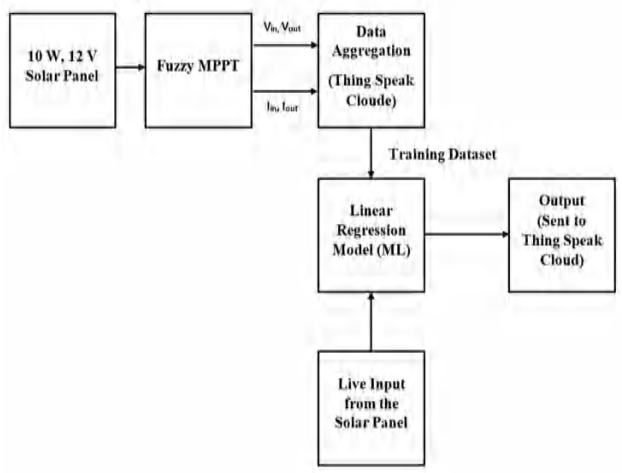

Figure 31: The block diagram for the Linear regression MPPT

6.3 Results and discussion

The python script for linear regression model is written in IDLE shell 3.9.2. The hardware setup and the output results in thingspeak server is shown in the Figure 32. The dataset used to train the linear regression model was recorded on June 22, 2022 from the fuzzy logic MPPT prototype.The python script and its results for linear regression model based MPPT algorithm are shown in the Figure 33. The input and the output profiles of voltage, current and power of linear regression based MPPT algorithm are shown in the Figure 34.

Figure 32: Hardware implementation of solar PV MPPT using linear regression machine learning algorithm

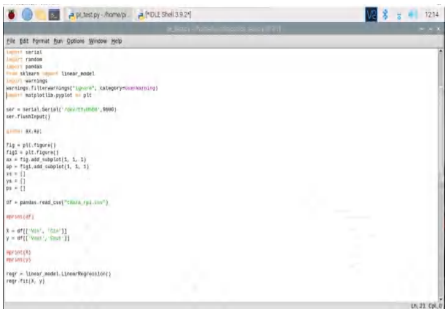

Figure 33: Python Script of Linear Regression Algorithm

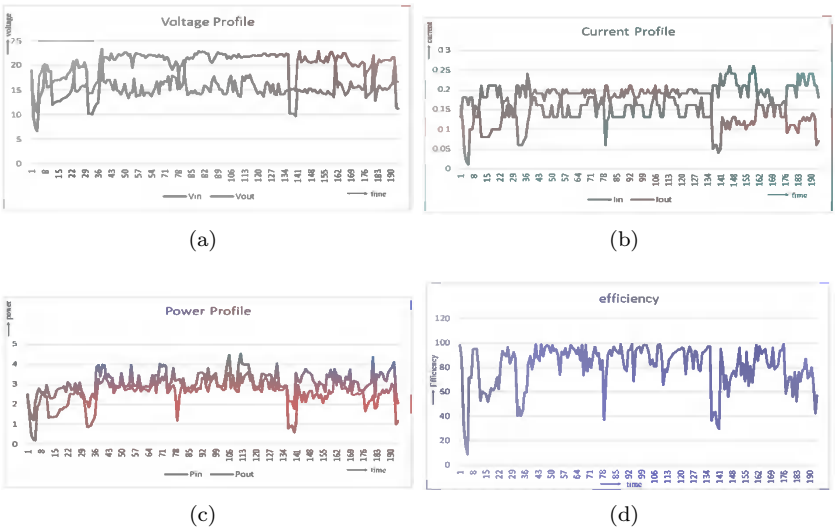

Figure 34: Response of the Solar PV system with Linear regression based MPPT algorithm a)Voltage profile, b)Current profile, c)Power profile, d)Efficieny

From the figure it is observed that when Vmp is between 15 V and 20 V, the buck-boost converter efficiency is greater than 80 % and when Vmp is less than 15 V, the converter efficiency is less than 60 %. To improve the tracking accuracy, the dataset of fuzzy MPPT needs to be increased. The limitation of the study is dataset collected using fuzzy logic MPPT algorithm for a day in month of June. The irradiance and temperature of the panel for a particular time of day varies based on the month and season of the year. A huge dataset are required for various months and seasons to make the regression model to best fit. Further accuracy of the algorithm can be improved by optimizing the regression coefficient of the model.

7 Conclusions

Cost management plays crucial role in grid connected renewable energy system. In this article MATLAB /Simulink simulations have been used to investigate MTDE algorithm for energy and cost management controllers in grid-connected domestic PV-wind systems linked with battery storage. Using a hybrid power system modelling model, Tamilnadu's hourly irradiance and wind speed profiles are analysed. The proposed hybrid system's energy management controller is analysed utilizing MTDE and GSA methodologies under a time-of-use tariff. In both algorithms, maximizing the cost benefit of the household is taken as the objective, and the dispatching ratio of electricity sold to the grid and used locally is treated as the optimisation variable. The performance of the proposed MTDE method is compared with that of the GSA and conventional self-made for self-consumed and rest for sale mode-based energy management controllers in the aspect of daily cost benefit.The daily cost benefit of the proposed system is Rs 16.898 while it is Rs 14.798 by GSA and Rs 12.183 by the SFC & RFS method. In comparison with the existing SFC & RFS method, GA analysed in the existing literature offered revenue growth rate of 17.74% while by the GSA analysed in this article, it is improved to 21.46%. The proposed MTDE revenue growth rate in comparison with the existing SFC & RFS method is 38.7% which is greater than both GA and GSA. Compared with the government-advocated SFC & RFS mode, the proposed MTDE-based strategy can indeed obtain maximum benefits through optimisation methodology.This means implementing the proposed system enhances both energy efficiency and the economic benefits for the end user. The efficiency of the solar PV system enhanced by using fuzzy logic MPPT controller which works well in changing irradiance and temperature with reduced oscillations near maximum power point. The experimentation is performed with a hardware protype which validates the performance of fuzzy MPPT with 5 input membership functions, 9 output membership functions and 25 fuzzy rule set and recorded 5.5 Watts at maximum power point voltage of 16.5 V. The tracking accuracy can be improved by increasing the membership functions and rule sets. The tracking time can be improved by introducing the machine learning techniques. The linear regression-based machine learning algorithm are trained using fuzzy logic MPPT data and implemented. The performance of the linear regression based MPPT inherits the characteristics of fuzzy logic MPPT with increased tracking time. It is observed that the mean square error (MSE) is 26.3521 and root mean square error (RMSE) is 5.1334. The performance of the model can be improved by increasing the training dataset and optimizing the regression coefficient. The accuracy of the model can be further improved by increasing the dataset

of fuzzy logic MPPT for various seasonal conditions. In this article, MTDE and GSA are analysed as energy and cost management controllers in grid-connected residential PV-wind generation systems coupled with battery storage. In future, the research may extend to fuel cells for industrial applications. Since Machine learning is capable for big data, in future research may extend with yearly data.

Acknowledgement

The authors wish to express their appreciation for several excellent suggestions for improvements in this paper made by the referees.

References

[1] U. Akram, M. Khalid, S. Shafiq, *An innovative hybrid wind-solar and battery-supercapacitor microgrid system-development and optimization*, IEEE Access, **5** (2017), 25897-25912. https://doi.org/10.1109/ACCESS.2017.2767618

[2] L. Ashok Kumar, A. Alexander, *Power electronic converters for solar photovoltaic systems*, Academic Press, Elsevier, 2020. https://doi.org/10.1016/C2019-0-04270-7

[3] M. A. E. S. Badr, *Modeling, simulation and optimization of wind farms and hybrid systems*, IntechOpen, (2020), 145-162.

[4] R. Banos, F. Manzano-Agugliaro, F. G. Montoya, C. Gil, A. Alcayde, J. Gómez, *Optimization methods applied to renewable and sustainable energy: A review*, Renewable and Sustainable Energy Reviews, **15**(4) (2011), 1753-1766.

[5] F. Cucchiella, P. Rosa, *End-of-Life of used photovoltaic modules: A financial analysis*, Renewable and Sustainable Energy Reviews, **47** (2015), 552-561. https://doi.org/10.1016/j.rser.2015.03.076

[6] I. Cvitić, D. Peraković, M. Periša, B. Gupta, *Ensemble machine learning approach for classification of IoT devices in smart home*, International Journal of Machine Learning and Cybernetics, **12**(11) (2021), 3179-202. https://doi.org/10.1007/s13042-020-01241-0

[7] M. Deveci, D. Pamucar, I. Gokasar, M. Köppen, B. B. Gupta, *Personal mobility in metaverse with autonomous vehicles using Q-rung orthopair fuzzy sets based OPA-RAFSI model*, IEEE Transactions on Intelligent Transportation Systems, (2022), 1-10. https://doi.org/10.1109/TITS.2022.3186294

[8] A. Ghodousian, F. S. Yousef, *Linear optimization problem subjected to fuzzy relational equations and fuzzy constraints*, Iranian Journal of Fuzzy Systems, **20**(2) (2023), 1-20. https://doi.org/10.22111/IJFS.2023.7552

[9] A. R. Gollou, N. Ghadimi, *A new feature selection and hybrid forecast engine for day-ahead price forecasting of electricity markets*, Journal of Intelligent and Fuzzy Systems, **32**(6) (2017), 4031-4045. https://doi.org/10.3233/JIFS-152073

[10] D. Gómez-Lorente, F. Aznar, O. Rabaza, *MPPT algorithm based on multiple linear regression model for solar PV systems*, 20th International Conference on Renewable Energies and Power Quality, **30** (2022), 100-105. https://doi.org/10.24084/repqj20.233

[11] M. Grace, C. Sunetra, *Optimal energy management of a grid-tied solar PV-battery microgrid: A reinforcement learning approach*, Energies, **14**(9) (2021), 2700. https://doi.org/10.3390/en14092700

[12] M. Hamian, A. Darvishan, M. Hosseinzadeh, M. J. Lariche, N. Ghadimi, A. Nouri, *A framework to expedite joint energy-reserve payment cost minimization using a custom-designed method based on mixed integer genetic algorithm*, Engineering Applications of Artificial Intelligence, **72** (2018), 203-212. https://doi.org/10.1016/j.engappai.2018.03.022

[13] N. Hemalatha, R. Seyezhai, *Implementation of fuzzy MPPT controller for PV-based three-phase modified capacitor-assisted extended boost q-ZSI*, Applied Nanoscience, **13**(3) (2023), 1971-1979. https://doi.org/10.1007/s13204-021-02025-w

[14] M. Hosseini Firouz, N. Ghadimi, *Optimal preventive maintenance policy for electric power distribution systems based on the fuzzy AHP methods*, Complexity, **21**(6) (2016), 70-88. https://doi.org/10.1002/cplx.21668

[15] R. Inglesi-Lotz, J. N. Blignaut, *Estimating the price elasticity of demand for electricity by sector in South Africa*, South African Journal of Economic and Management Sciences, **14**(4) (2011), 449-465.

[16] I. Kouatli, *Fuzziness control of fuzzimetric sets*, IEEE International Conference on Fuzzy Systems, (2019), 1-5. https://doi.org/10.1109/FUZZ-IEEE.2019.8858828

[17] Y. Liu, W. Wang, N. Ghadimi, *Electricity load forecasting by an improved forecast engine for building level consumers*, Energy, **139** (2017), 18-30. https://doi.org/10.1016/j.energy.2017.07.150

[18] F. Mirzapour, M. Lakzaei, G. Varamini, M. Teimourian, N. Hadimi, *A new prediction model of battery and wind-solar output in hybrid power system*, Journal of Ambient Intelligence and Humanized Computing, **10**(1) (2019), 77-87. https://doi.org/10.1007/s12652-017-0600-7

[19] M. H. Nadimi-Shahraki, S. Taghian, S. Mirjalili, H. Faris, *MTDE: An effective multi-trial vector-based differential evolution algorithm and its applications for engineering design problems*, Applied Soft Computing Journal, **97** (2020), 106761. https://doi.org/10.1016/j.asoc.2020.106761

[20] K. Rafeeq Ahmed, K. Farrukh Sayeed, K. Logavani, T. J. Catherine, R. Shimpy, R. Mahesh Singh, R. Thandaiah Prabu, B. Bala Subramanian, Adane Kassa, *Maximum power point tracking of PV grids using deep learning*, International Journal of Photoenergy, (2022). https://doi.org/10.1155/2022/1123251

[21] M. M. Rahman, S. Hettiwatte, G. M. Shafiullah, A. Arefi, *An analysis of the time of use electricity price in the residential sector of Bangladesh*, Energy Strategy Reviews, **18** (2017), 183-198. https://doi.org/10.1016/j.esr.2017.09.017

[22] E. Rashedi, H. Nezamabadi-pour, S. Saryazdi, *GSA: A gravitational search algorithm*, Information Sciences, **179**(13) (2009), 2232-2248. https://doi.org/10.1016/j.ins.2009.03.004

[23] N. Sampathraja, L. Ashok Kumar, *Analysis of energy management controller in grid-connected PV wind power system coupled with battery using whale optimisation algorithm*, Iranian Journal of Science and Technology, Transactions of Electrical Engineering, **46**(1) (2022), 77-90. https://doi.org/10.1007/s40998-021-00469-y

[24] J. R. San Cristóbal, *A goal programming model for the optimal mix and location of renewable energy plants in the north of Spain*, Renewable and Sustainable Energy Reviews, **16** (2012), 4461-4464. https://doi.org/10.1016/j.rser.2012.04.039

[25] M. R. Setayandeh, A. R. Babaei, *A novel method for multi-objective design optimization based on fuzzy systems*, Iranian Journal of Fuzzy Systems, **18**(5) (2021), 181-198. https://doi.org/10.22111/IJFS.2021.6264

[26] S. Sumathi, S. Rajappa, L. Ashok Kumar, S. Surekha, *Advanced decision sciences based on deep learning and ensemble learning algorithms*, Nova Science Publishers, 2021.

[27] R. K. Swain, N. C. Sahu, P. K. Hota, *Gravitational search algorithm for optimal economic dispatch*, Procedia Technology, **6** (2012), 411-419. https://doi.org/10.1016/j.protcy.2012.10.049

[28] S. Zhang, Y. Tang, *Optimal schedule of grid-connected residential PV generation systems with battery storages under time-of-use and step tariffs*, Journal of Energy Storage, **23** (2019), 175-182. https://doi.org/10.1016/j.est.2019.01.030